Opposite Page:

Electron micrographs of silicon microcombs. Teeth are ~500 mm wide. a) Spring comb. b) Reference comb.
Courtesy of N. Butler, C. Chen, W. Gu, Dr. R. Heilmann, P. Konkola, O. Mongrard, G. Monnelly
(C. R. Canizares, G. R. Ricker, and M. L. Schattenburg)
Research sponsored by NASA and GSFC

Submicron and Nanometer Structures

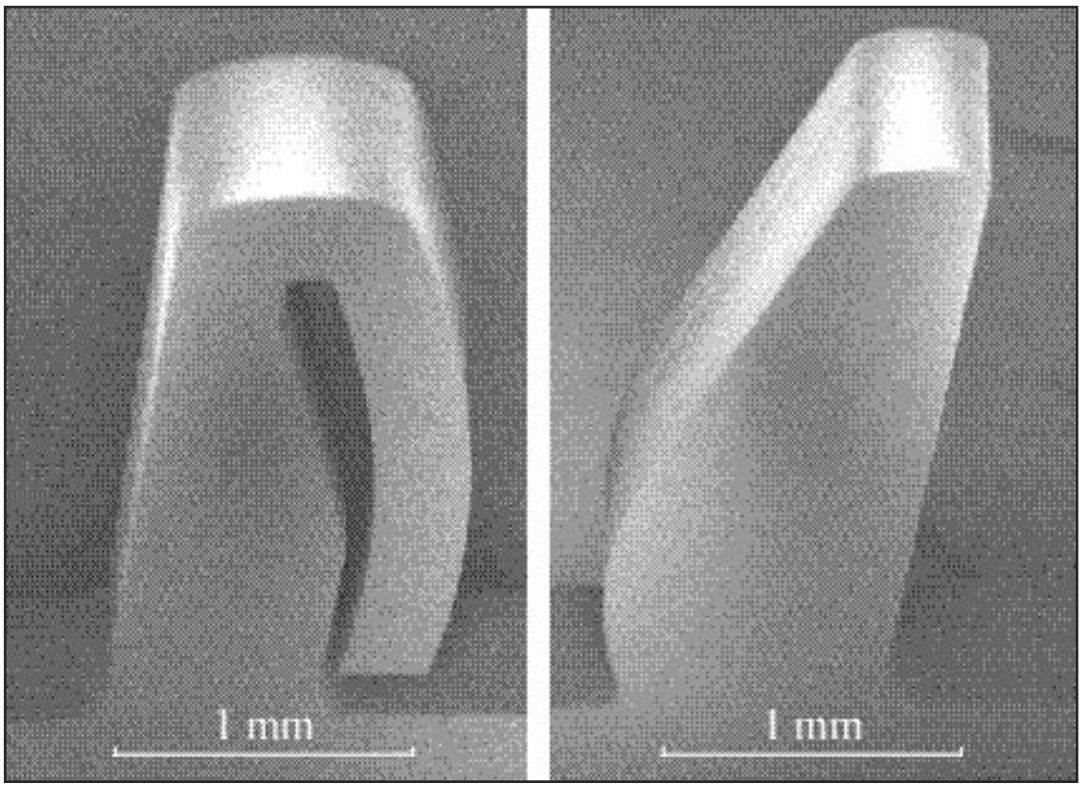

Submicron and Nanometer Structures

- *Magnetic Random Access Memories (MRAMs)*
- *Magnetic Anisotropy and Microstructure in Cr/CoCrPtTa Hard Disk Films*
- *Super-smooth X-ray Reflection Gratings*
- *UV-blocking Transmission Gratings Filters for Neutral Atom Imaging*
- *Transmission Gratings for X-ray and Atom-Beam Spectroscopy and Interferometry*
- *High-Dispersion X-ray Transmission Gratings for Space Research*
- *High-Accuracy Assembly of X-ray Foil Optics*
- *Resonant Raman Spectra from One Carbon Nanotube*
- *Electronic Properties of Bismuth Nanowires*
- *Nanomagnets*
- *Magnetic and Optical Films made by Pulsed Laser Deposition*
- *Low Voltage Field Emitter Arrays by Aperture Scaling*

layer. To read, a smaller current is passed, which can change the magnetization of the soft layer only. The resistance of the element depends on whether the hard and soft layers are magnetized parallel or antiparallel, hence changes in the resistance resulting from the reversal of the soft layer can be used to probe the magnetic state of the hard layer. Elements are arranged in a rectangular array and connected with conductor lines, allowing individual elements to be selected.

We have used interference lithography combined with ion-milling to produce arrays of Co/Cu/NiFe spin-valve elements and prototype MRAM devices. The aim of this research is to investigate the behavior of sub-100 nm elements, much smaller than those used in present-day MRAM devices. We find that the switching of the individual Co and NiFe layers is preserved, and the elements show single-domain behavior. The magnetic behavior at these size scales is dominated by magnetostatic interactions between the two layers.

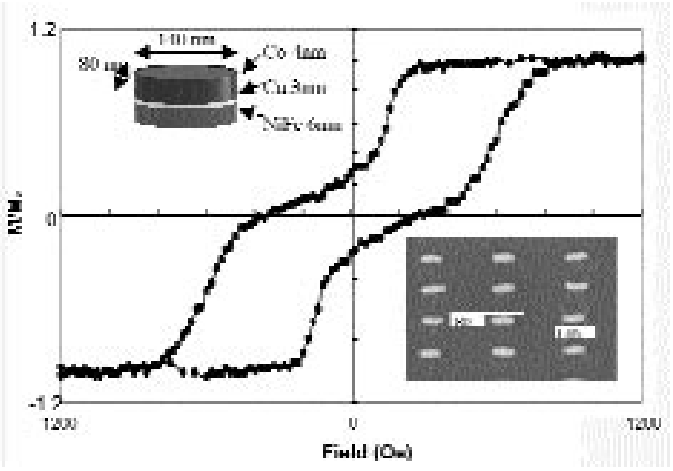

Fig. 2: Hysteresis loop of an array of 80 nm x 140 nm elliptical particles made of a Co/Cu/NiFe film. The steps in the loop correspond to the separate switching of the NiFe and Co layers, which are coupled antiparallel at remanence.

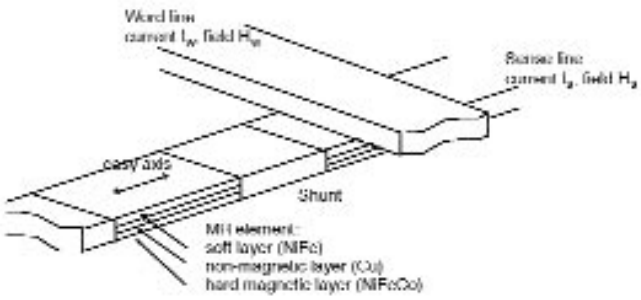

Fig. 1: Schematic of MRAM structure, which consists of an array of parallel sense lines and parallel word lines. The MR elements are connected in series. Magnetic fields generated by currents passed simultaneously through a sense line and a word line write the element at the intersection of the two lines. To read, resistance changes in the sense line caused by a smaller wordline current are measured.

Continued

Continued

Personnel

B. Vogeli, F. Castano, M. Walsh, Y. Hao, and S. Haratani (C.A. Ross and H.I. Smith in collaboration with J.Q. Wang)

Sponsorship

TDK Corp. and DARPA through U. of New Orleans

MRAMs are solid-state non-volatile magnetic storage devices in which each bit of data is stored an a small, elongated magnetoresistive sandwich element. A typical MagnetoResistive (MR) sandwich consists of two magnetic layers of different coercivity, one hard and one soft.

The direction of magnetization of the hard layer is used to represent the data bit. To write data, a magnetic field is applied by passing a current through a conductor line (word line) adjacent to the element, such that the field is large enough to change the magnetization of the hard

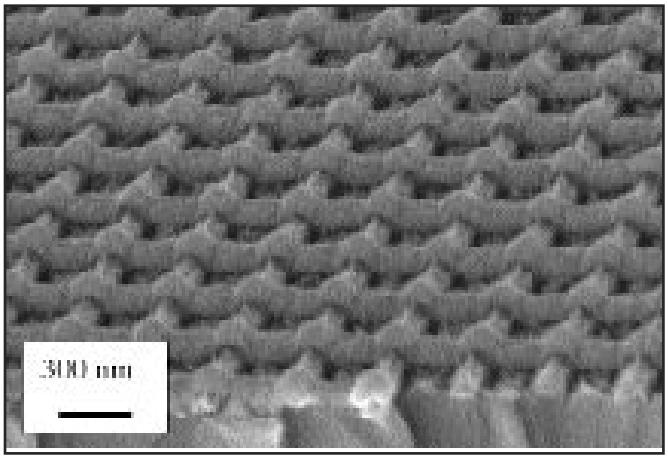

Fig. 3: A prototype MRAM device. The horizontal lines are the 'word' lines, while the lines running nearly vertically are the sense lines. At each intersection there is a 100nm x 150 nm MRAM element. The cell size is 300 nm x 400 nm.

Magnetic Anisotropy and Microstructure in Cr/CoCrPtTa Hard Disk Films

Personnel

D. Twisselmann, P. Chambers, and E. Siem (C.A. Ross)

Sponsorship

NSF and National Storage Industries Consortium

Magnetic CoCrPtTa films on a Cr underlayer are used in hard disks to store data. The films are deposited at temperatures of 200˚C or above, which causes the b.c.c. Cr to grow with a (200) crystallographic texture. The hexagonal Co alloy grows epitaxially on the Cr with a (11.0) texture, putting its c-axis parallel to the film plane. In such films, the presence of substrate roughness has significant effects on in-plane magnetic anisotropy. In particular, the presence of grooves or scratches in the substrate causes the coercivity, remanence and squareness of the film to be considerably higher parallel to the grooves compared to their values in the perpendicular direction. This effect is useful in hard disks, but the physical origin of this anisotropy is still debated. It may be due to in-plane stress differences between the circumferential and radial directions, to preferential orientation of the Co-alloy c-axes along the grooves, or to differences in magnetostatic coupling.

We have measured the anisotropy in films deposited onto oxidised silicon substrates with well-controlled submicron surface topography, to explore the origins of the effect and to demonstrate how it can be enhanced by choice of substrate features. Substrates are patterned with shallow, parallel grooves, then coated with Cr/CoCrPt films. Both the stress in the films, and the preferred c-axis orientation, have been characterized, and related to the measured in-plane anisotropy. We find that magnetostrictive effects, due to the biaxial stress state of the Co-alloy films, account for about 1/4 of the measured anisotropy. The majority of the anisotropy, however, is caused by a preference for the Co c-axes to lie parallel to the grooves. This is thought to be a result of preferential nucleation of certain Co variants on the Cr underlayer, because the Cr is itself in a biaxial strain state. We have also been investigating the nucleation and growth of these Co and Cr films, to help understand their morphology and to control grain size for high-density media.

Continued

Continued

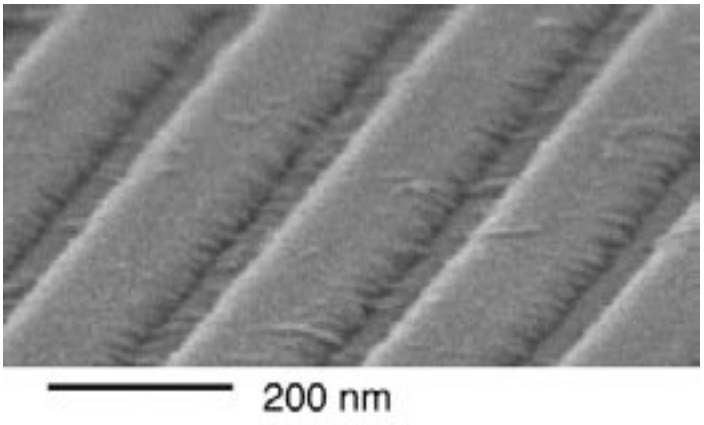

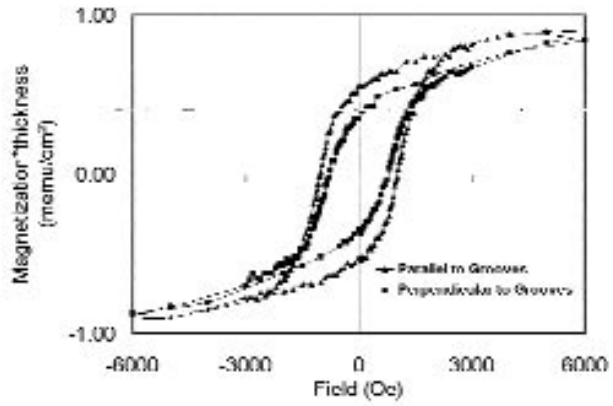

Fig 4: Magnetic hysteresis loops from a sample of Cr/CoCrPt sputtered onto a substrate with 200 nm period, 20 nm deep grooves. Coercivity, remanence and squareness are higher parallel to the grooves (solid line) compared to perpendicular (dotted).
Top: Example of a film sputtered on a grooved substrate.

Super-smooth X-ray Reflection Gratings

Personnel

R. C. Fleming, Dr. R. Heilmann, E. Murphy
(M. L. Schattenburg, C. R. Canizares and H. I. Smith)

Sponsorship

NASA and Columbia University (NASA)

Grazing-incidence X-ray reflection gratings are an important component of modern high-resolution spectrometers and related X-ray optics. These have traditionally been fabricated by diamond scribing with a ruling engine, or more recently, by interference lithography followed by ion etching. These methods result in gratings which suffer from a number of deficiencies, including high surface roughness and poor groove profile control, leading to poor diffraction efficiency and large amounts of scattered light.

We are developing improved methods for fabricating blazed X-ray reflection gratings which utilize special (111) silicon wafers, cut ~1 degree off the (111) plane. Silicon anisotropic etching solutions, such as potassium hydroxide (KOH), etch (111) planes extremely slowly compared to other crystallographic planes, resulting in the desired super-smooth blaze surface. Previous work used similar off-cut (111) silicon substrates to fabricate blazed diffraction gratings. However, that method utilized a second KOH etch step that compromised the grating facet flatness and is unsuitable for small grazing-angle X-ray diffraction.

Our gratings are patterned using interference lithography with the λ=351.1 nm wavelength, and transferred into the substrate using tri-level resist processing, Reactive-Ion Etching (RIE), and silicon-nitride masking during the KOH etch. The narrow (~100 nm) ridge of silicon which supports the nitride mask is removed using a novel chromium lift-off step followed by a CF4 RIE trench etch. The result is extremely-smooth sawtooth patterns, which, after applying a thin evaporative coating of Cr/Au, are suitable for X-ray reflection (see Figure 5). Gratings have been tested with special X-ray spectrometers in the laboratories of our collaborators at Columbia University and the Lawrence Berkeley Laboratory. Peak gratings efficiencies achieved are ~35% greater than those of the best available ruled masters of comparable design (see Figure 6).

Continued

Continued

Potential applications of these improved gratings are for synchrotron studies and satellite-based high-resolution X-ray spectroscopy for planned NASA missions such as Constellation X. The current phase of the work involves patterning gratings on super-flat wafers, and trimming the substrates into the desired rectangular format.

Fig. 5: (a) An AFM image of a traditional mechanically-ruled and replicated X-ray reflection grating (Bixler et al., Proc. SPIE 1549, 420-428 [1991]). Note the rough, wavy grating surfaces that lead to poor diffraction performance. (b) An AFM image of a blazed X-ray reflection grating fabricated by anisotropic etching of special off-cut (111) silicon wafers. Note the improvement of grating surface flatness and smoothness, leading to significantly improved performance.

Fig. 6: Comparison of X-ray diffraction efficiency measured at Lawrence Berkeley Laboratory and electromagnetic finite element calculations performed at Columbia University. Peak gratings efficiencies achieved are ~35% greater than those of the best available ruled masters of comparable design.

UV-blocking Transmission Gratings Filters for Neutral Atom Imaging

Personnel

J. Carter, R. C. Fleming, and E. Murphy
(M. L. Schattenburg, C. R. Canizares, and H. I. Smith)

Sponsorship

LANL and SwRI

Neutral-atom-beam imaging detectors are used to study dilute plasmas in astrophysical environments such as the magnetospheric regions of the Earth and other planets, and laboratory systems such as Tokamaks. Neutral atom emission can be a particularly useful probe of plasmas since neutrals travel in straight lines-of-sight, unperturbed by electromagnetic fields.

Charge-exchange interactions between Solar-wind particles and atoms in the Earth's tenuous outer atmosphere are predicted to form strong currents of neutral atoms (mostly oxygen and helium) emanating from the Earth, which, if they could be imaged, would provide unprecedented real-time mapping of this complicated magnetohydrodynamic environment. This information would be valuable in order to safeguard the health of orbiting satellites, and ensure the stability of our nation's electric power grid.

Unfortunately, sensitive orbiting neutral-beam detectors are easily overwhelmed by the bright flux of UV photons typically emitted from astrophysical plasmas (mostly the λ=121.6 nm emission from hydrogen and the 58.4 nm emission from helium). Filters that allow the passage of low-energy neutral atoms but block UV light are essential for the performance of this instrumentation (see Figure 7). Through several years of collaboration with the Los Alamos National Laboratory (LANL), the University of West Virginia, the University of Southern California, and the Southwest Research Institute (SwRI), we have developed neutral beam filters which consist of mesh-supported, 200 nm-period, gold transmission gratings with 30-60 nm wide slots (Figure 8). The tall, narrow slots in the gratings behave as lossy waveguides at or below cutoff, providing UV discrimination to particles on the order of millions.

The SNL was awarded contracts by SwRI and LANL to deliver a quantity of flight grating filters for the *Medium Energy Neutral Atom* (MENA) instrument on the NASA *Magnetospheric Imaging Medium-Class Explorer* (IMAGE) mission, launched March 25, 2000, and improved gratings for the NASA *Two Wide-Angle Imaging Neutral-atom Spectrometers* (TWINS A, B) Missions.

Gratings are fabricated by interference lithography with tri-level resist, followed by cryogenic reactive-ion etching and gold electroplating. Additional masking steps

Fig. 7: Concept of UV filtering by means of a metal freestanding grating. As a result of polarization and waveguide effects, UV is blocked while allowing the passage of atoms. In this way, UV background counts on the atom detector are avoided.

Continued

Continued

followed by nickel plating fabricate the mesh support structure, and a chemical etching step yields mesh-supported gratings suitable for space use. Additional processing is required to align and bond the gratings to frames.

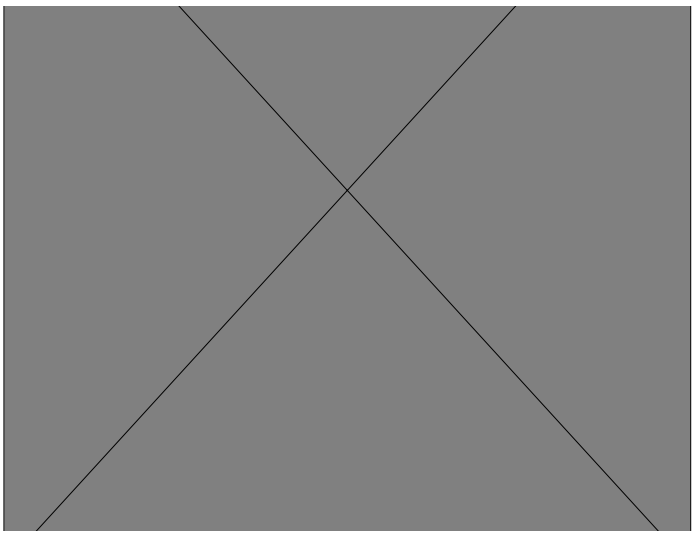

Fig. 8: Scanning-electron micrograph image of a UV blocking grating. Due to the narrow slot width of 30-35 nm, as shown in the picture, and the large slot depth (~500 nm), the UV transmission is extremely low (10^{-6} to 10^{-7} at λ=121.6 nm), while decreasing the transmitted atomic flux by only a factor of 10.

Transmission Gratings for X-ray and Atom-Beam Spectroscopy and Interferometry.

Personnel

T. A. Savas, J. M. Carter, and E. Murphy
(M. L. Schattenburg and H. I. Smith)

Sponsorship

X-OPT, Inc.

Transmission gratings with periods of 100 to 1000 nm are finding increasing utility in applications such as X-ray, vacuum-ultraviolet, and atom-beam spectroscopy and interferometry. Over 30 laboratories around the world depend on MIT-supplied gratings in their work. For X-ray and VUV spectroscopy, gratings are made of gold and have periods of 100 to 1000 nm, and thicknesses ranging from 100 to 1000 nm. The gratings are most commonly used for spectroscopy of the X-ray emission from high-temperature plasmas. Transmission gratings are supported on thin (1 micron) polyimide membranes, or made self supporting ("free standing") by the addition of crossing struts (mesh). (For short X-ray wavelengths, membrane support is desired, while for the long wavelengths, a mesh support is preferred in order to increase efficiency.) Fabrication is performed by interference lithography combined with reactive-ion etching and electroplating. Progress in this area tends to focus on improving the yield and flexibility of the fabrication procedures.

Another application is the diffraction of neutral-atom and molecular beams by mesh supported gratings. Lithographic and etching procedures have been developed for fabricationg free-standing gratings and grids in thin silicon nitride (SiN_x) membranes supported in a Si frame. Figure 9 shows a free-standing 100 nm period grating in 100 nm-thick silicon nitride. Figure 10 shows a 100 nm-period grid in a 100 nm-thick SiN_x membrane. Such a grid is used in experiments as a "molecular sieve."

We have established a collaboration with the Max-Planck Institute in Göttingen, Germany, in which they utilize our gratings of 100 nm period in diffraction experiments using atomic, molecular, and helium-cluster beams.

As shown in Figure 11 the diffraction of atomic and molecular beams reveals striking deviations from Kirchhoff's optical diffraction theory. The analysis of

Continued

the diffraction intensities allowed for a quantitative determination of the attractive atom(molecule)-surface van der Waals interaction at the silicon nitride surface for various atomic and molecular species including He, Ne, Ar, Kr, He*, Ne*, D_2, and CH_3F. The diffraction of cluster beams by a transmission grating has been established as a unique technique for the non-destructive mass selection and detection of small and weakly bound van der Waals clusters. Recently, the Göttingen group discovered bound states in mixed-isotope helium clusters, e.g. $^3He^4He_2$, $^3He^4He_3$, etc., by diffraction from one of our 100-nm-period gratings as shown in Figure 12. In addition, they employed the grating to measure the bond length of the helium dimer, $^4He_2$, which is assumed to be the weakest molecular bond. Further experiments based on the transmission gratings include the study of cluster formation dynamics and the search for the Efimov effect in the helium trimer.

Data obtained by helium-atom-beam diffraction at large incident angles showed Lyman ghosts in the spectrum. This data led to the development of new fabrication techniques to improve the quality of the free-standing gratings in silicon nitride. Diffraction spectra from gratings made with the improved process show no Lyman ghosts, illustrating the important synergy between applications and nanofabrication.

Highly successful diffraction experiments with beams

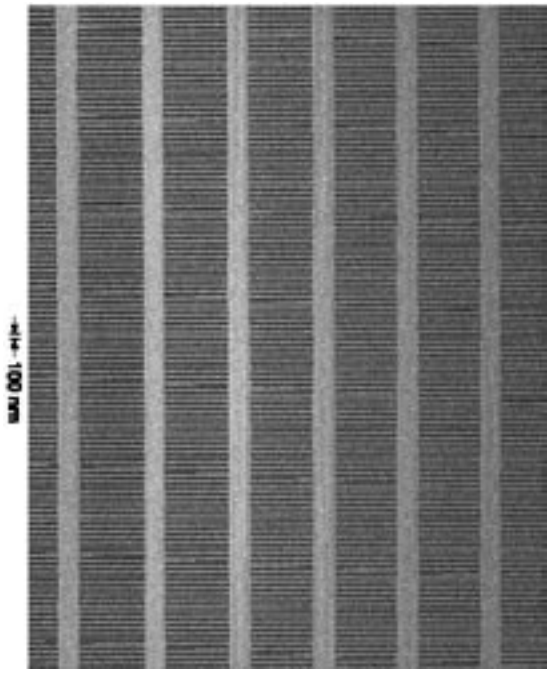

Fig 9: Scanning electron microgrph of a free-standing 100 nm-period grating (50 nm-wide bars) in a silicon nitride membrane of area 500 microns by 5 mm.

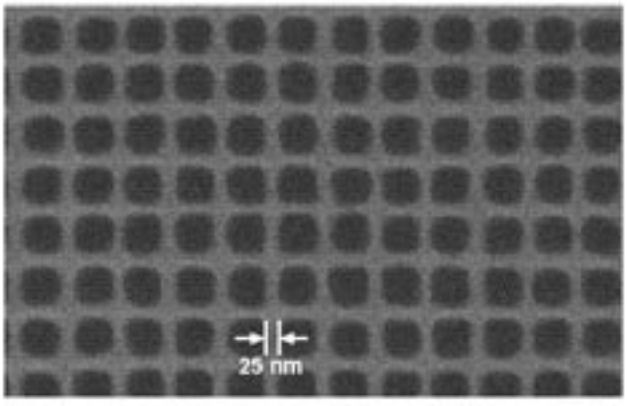

Fig. 10: Scanning electron micrograph of a free-standing 100 nm period grid in a silicon nitride membrane of area 500 micron by 5 mm. Such grids are used in experiments to separate out Helium trimers from other clusters.

Continued

of buckyballs (C60) have been carried out with our 100 nm-period, free-standing SiNx gratings by Dr. Markus Arndt of the University of Vienna.

Our 100 nm-period free-standing SiNx gratings are also used for atom interferometry by two groups: those of Prof. David Pritchard of MIT and Prof. Bruce Doak of the State University of Arizona. Pritchard's group interferes neutral beams of sodium atoms while Doak's group interferes helium beams (performed at the Max Planck Institute in Göttingen, Germany in collaboration with P. Toennies).

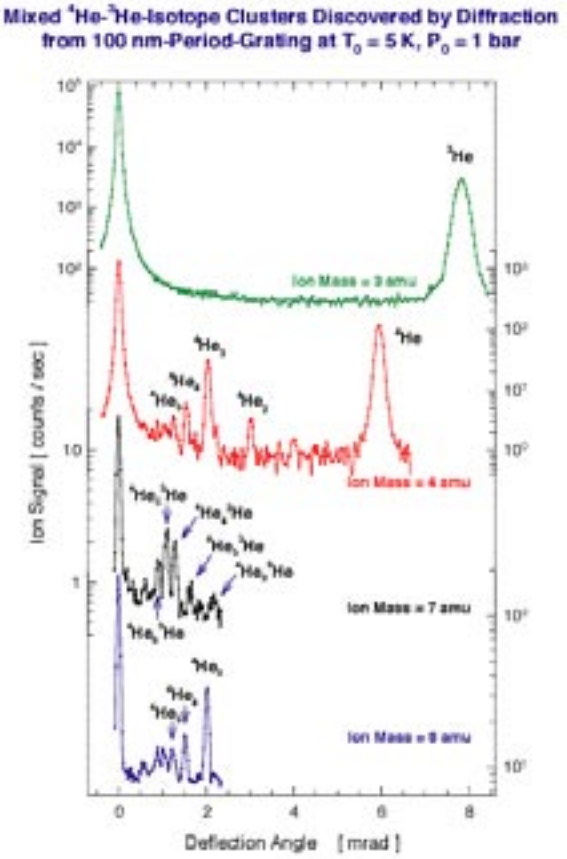

Fig. 11: Rare-gas atom-beam diffraction patterns. These results were obtained by Wieland Schöllkopf and Peter Toennies at the Max-Planck Institute in Göttingen, Germany, using a free-standing, 100nm-period grating.

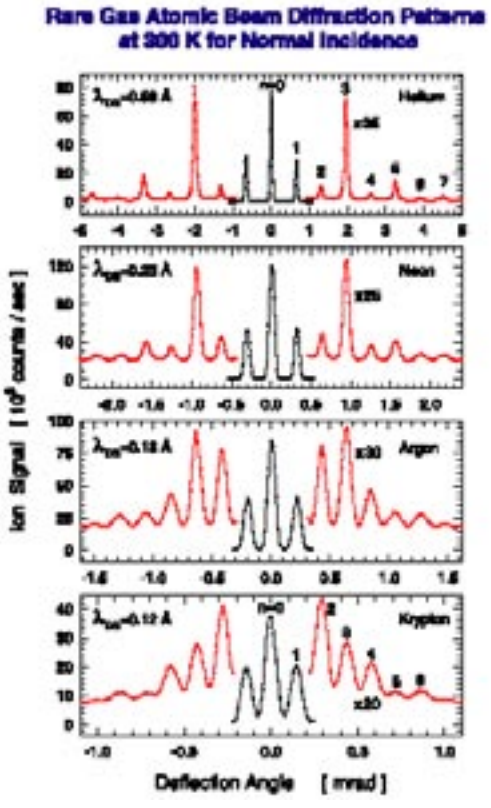

Fig. 12: Non-destructive mass separation of small mixed-isotope helium clusters. These results were obtained by Wieland Schöllkopf and Peter Toennies at the Max-Planck Institute in Göttingen, Germany, using a free-standing, 100nm-period grating.

High-Dispersion X-ray Transmission Gratings for Space Research

Personnel

J. Carter, R. C. Fleming, and E. Murphy
(M. L. Schattenburg, C. R. Canizares and H. I. Smith)

Sponsorship

NASA and NOAA (through XOPT Inc.)

High-dispersion X-ray and EUV transmission gratings are fabricated for space missions including the *Solar EUV Monitor* (SEM) on the NASA *Solar and Heliospheric Observatory* (SOHO) mission, launched December 2, 1995, the NASA *Chandra* X-ray telescope, launched July 23, 1999, and the NOAA Geostationary Operational Environmental Satellites (GOES N, O, P, Q) missions. The *Chandra* telescope provides high-resolution imaging and spectroscopy of X-ray-emitting astrophysical objects, with unprecedented power and clarity, which is significantly widening our view of the Universe. The SOHO and GOES satellite series perform solar Extreme UltraViolet (EUV) monitoring which provides early warning of solar flare events that could imperil satellite and astronaut operations.

Many hundreds of large-area, gold transmission gratings, with 200 nm and 400 nm periods, were required for the High-Energy-Transmission-Grating Spectrometer (HETGS) on *Chandra*, which provides high-resolution X-ray spectroscopy in the 100 eV to 10 keV band (see Figure 13). In order to achieve spectrometer performance goals, the gratings need to have very low distortion (<200 ppm) and high-aspect-ratio structures, significantly pushing the state-of-the-art of nanofabrication (see Figure 14). While the *Chandra* gratings were fabricated on thin (<1.0 μm) polymer membranes, the SOHO and GOES gratings need to be freestanding to transmit the softer solar spectrum, and are supported instead by a lithographically-patterned nickel mesh. The need for high grating quality, and tight production deadlines, demand a robust, high-yield manufactur-

Fig. 13: Photograph of the HETGS flight instrument on the Chandra X-ray telescope, which consists a 1.0 meter-diameter aluminum wheel populated with hundreds of 200 nm and 400 nm-period gold X-ray transmission gratings (340 total).

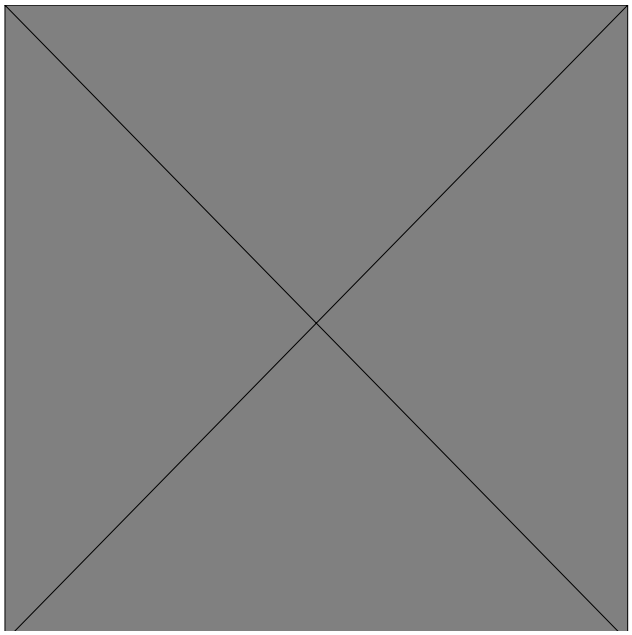

Fig. 14: Scanning-electron micrograph of a 200 nm-period HETGS gold X-ray transmission grating, cleaved to show line sidewalls.

Continued

ing process. Gratings are fabricated by interference lithography with tri-level resist, followed by cryogenic reactive-ion etching and gold electroplating. Additional masking steps followed by nickel plating fabricate the mesh support structure, and a chemical etching step yields mesh- or membrane-supported gratings suitable for space use. Additional processing is required to align and bond the gratings to frames. A simplified depiction of the process for fabricating membrane-supported gratings is shown in Figure 15. The *Space Nanotechnology Laboratory* (SNL) has extensive facilities for high-yield volume production of transmission gratings. Gratings undergo extensive testing before assembly into space instrumentation.

Fig. 15: Simplified depiction of HETGS grating fabrication process.

High-Accuracy Assembly of X-ray Foil Optics

Personnel

N. Butler, C. Chen, W. Gu, Dr. R. Heilmann, P. Konkola, O. Mongrard, and G. Monnelly
(C. R. Canizares, G. R. Ricker, and M. L. Schattenburg)

Sponsorship

NASA and GSFC

Future X-ray astronomy missions will require orders of magnitude improvements in collecting area and resolution. Foils optics are attractive candidates for telescope optics because of the tremendous weight and cost savings which can be achieved compared to traditional monolithic optics. However, substantial improvements in our ability to form and assemble foils to high accuracy are required. In this new research initiative we are developing a variety of microlithographic structures to shape and assemble foil optic components, both reflective and diffractive.

Silicon Micro-Optical-Mechanical Systems (MOMS) technology is used to lithographically fabricate silicon microstructures designed to guide and register glass foils into precise three-dimensional shapes with submicron accuracy. Thousands of ~200 μm-thick foils are typically required in an X-ray telescope, each shaped and assembled to form the precise polynomial curves that focus X-rays by grazing-incidence reflection. Figure 16 shows SEM images of two types of microcombs under development.

A prototype flight mirror structure based on these principles has been built and tested. Test results show that glass sheets are assembled to an accuracy of <0.5 microns, corresponding to an angle error of <1 arcsecond. This accuracy exceeds previous foil assembly methods by a factor of ~100. This breakthrough allows for the first time a foil optic telescope design with resolution comparable to the Chandra X-ray telescope (~1 arc-second) but with >10X larger collecting area and dramatically reduced weight and cost.

This microstructure assembly technology is supported by NASA for possible inclusion in the Constellation X telescope.

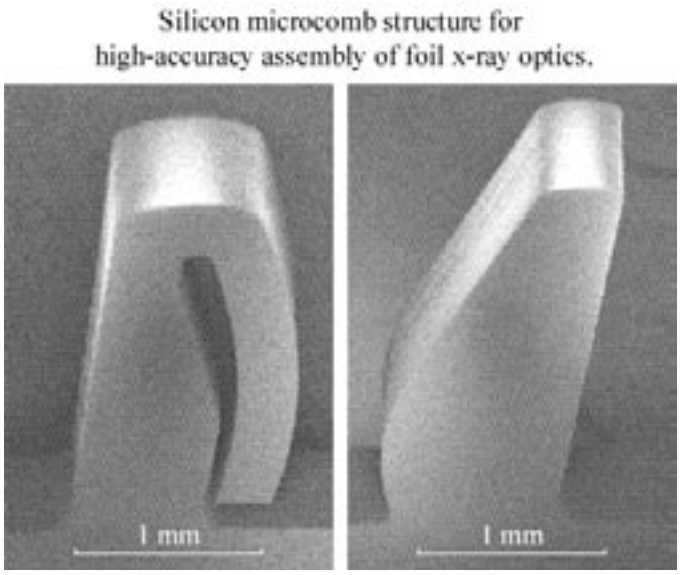

Fig. 16: Electron micrographs of silicon microcombs. Teeth are ~500 µm wide. a) Spring comb. b) Reference comb.

Resonant Raman Spectra from One Carbon Nanotube

Personnel

A. Jorio, A.G. Sousa Filho, S.D.M. Brown, K. Kneipp, M. A. Pimenta, J. H. Hafner, C. M. Leiber, G. Dresselhaus, and M. S. Dresselhaus

Sponsorship

NSF

The major breakthrough of our carbon nanotube research has been the recent observation of Raman spectra from one isolated Single Wall carbon Nanotube (SWNT), making possible its structural characterization, and the subsequent measurement of important physical properties on nanotubes of known structures. Experimentally, the research was facilitated by the availability of isolated single wall carbon nanotubes prepared by a chemical vapor deposition method developed in Professor Lieber's laboratory at Harvard University (see Figure 17). The structure of each single wall carbon nanotube is specified by its diameter and chiral angle, which are uniquely determined by two indices *(n,m)*. Because of the unique relation between the electronic structure and the *(n,m)* indices, we have been able to non-destructively determine the *(n,m)* structural indices of metallic and small diameter semiconducting single wall carbon nanotubes by measuring their Radial Breathing Mode (RBM) frequencies (see Figure 18). This finding will allow other researchers to measure various properties on nanotubes characterized for their *(n,m)* integers. This is important because of the sensitive dependence of these physical properties on *(n,m)*, as for example, nanotubes are metallic if $|n\text{-}m| = 3q$ and semiconducting if $|n\text{-}m| \pm 1 = 3q$. The observation of Raman spectra from one nanotube is possible because of the very large density of electronic states close to the van Hove singularities of these one-dimensional systems, so that under resonance Raman

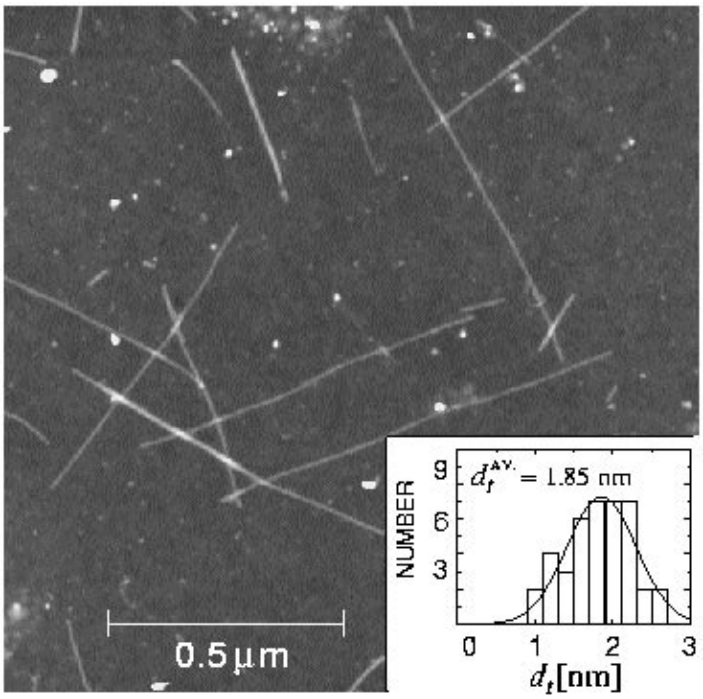

Fig. 17: Atomic force microscopy images of the sample. The inset shows the SWNT diameter distribution.

Continued

Continued

conditions when the incident or scattered photons are in resonance with an electronic transition between these van Hove singularities, strong coupling can occur between the electrons and phonons of the nanotube. One important property that we have ourselves studied by resonant Raman spectroscopy is the spectral profile of the joint density of states near a van Hove singularity. Many other physical properties are very sensitive to this spectral profile, but it is difficult to measure this profile directly, because probes such as scanning microscopy tips interact too strongly with the nanotube, thereby broadening the van Hove singularities.

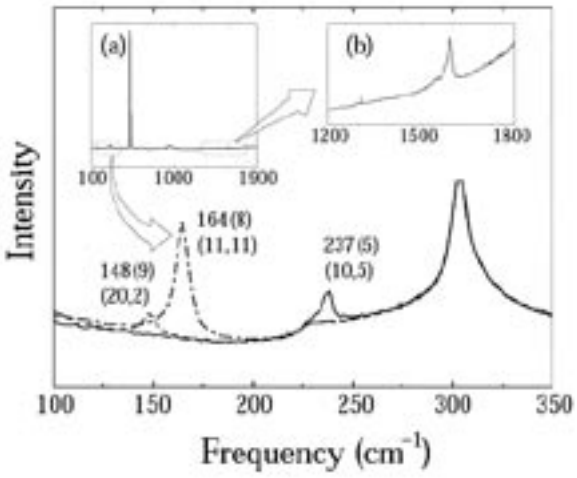

Fig. 18: Raman spectra come from three different spots on the Si substrate, showing the presence of only one resonant nanotube and one RBM frequency for each of 3 spots. The RBM frequencies (widths) and the (n,m) assignment for each resonant SWNT are displayed. The 303cm^{-1} feature comes from the Si substrate. Inset (a) shows the Raman spectra from one spot on the sample, including 303, 521 and 963cm^{-1} Raman features from the Si substrate. Inset (b) shows a zoom of the corresponding tangential mode G-band region.

Electronic Properties of Bismuth Nanowires

Personnel

S. B. Cronin, Y.-M. Lin, O. Rabin, M. R. Black, J. Heremans, J.Y. Ying, P. Gai, M.K. Mondol, H.I. Smith, G. Dresselhaus, and M. S. Dresselhaus

Sponsorship

US Navy, ONR MURI, and NSF

We have successfully fabricated arrays of bismuth nanowires with narrow diameter distributions, which can be varied between 7-200nm and can be made up to 100μm in length (see Figure 19). The nanowire arrays are produced using a non-lithographic fabrication technique of filling an electrochemically grown anodic alumina template with molten Bi. The Bi crystallizes with the same crystallographic structure as bulk Bi with wire densities of about $10^{10}/\text{cm}^2$. The crystalline direction along the nanowire axis is (012) for wire diameters < 50nm and (101) for diameters > 50nm. Bi wires doped with varying concentrations of the *n*-type dopant Te and of the isoelectric dopant Sb have also been fabricated. Substantial progress has been made in synthesizing bismuth nanowire arrays for thermoelectric applications within the pores of anodic alumina templates, especially for wires of small diameter. Figure 19 shows the SEM (Scanning Electron Microscopy) image of an alumina template with pore diameters of 20nm. A method has also been developed to grow much larger size arrays by using a silicon substrate.

Bismuth nanowires are of particular interest from a scientific standpoint because they undergo a semimetal-to-semiconductor transition as the wire diameter decreases below a critical diameter, d_c. The semimetal-to-semiconductor transition arises from quantum confinement effects in bismuth, which is a semimetal in bulk form. Quantum confinement causes the lowest *L* point conduction subband edge to move up in energy and the highest *T* point valence subband edge to move down, thus yielding a One-Dimensional (1D) semiconductor below some critical nanowire diameter d_c. Because of the very small effective mass of the carriers in bismuth, quantum effects are observed at larger wire diameters than for other materials. These special properties also make bismuth nanowires attractive for various nanoscale applications.

I-V measurements have been made both on wire arrays in the templates and on individual Bi nanowires that have been removed from the alumina template. In

Continued

this measurement on the individual wires, a pattern of four electrodes is affixed on top of a single Bi nanowire using electron beam lithography, and the facilities available in Professor H.I. Smith's NanoStructures Laboratory (NSL). Progress with these measurements has been hampered by the rapid formation of a high resistivity oxide coating on the bismuth nanowires, as shown in Figure 20. The oxide has been significantly reduced by annealing the samples in a hydrogen environment and also by sputtering off the oxide using FIB (Focused Ion Beam) milling and the facilities of Prof. C. Lieber's laboratory at Harvard University.

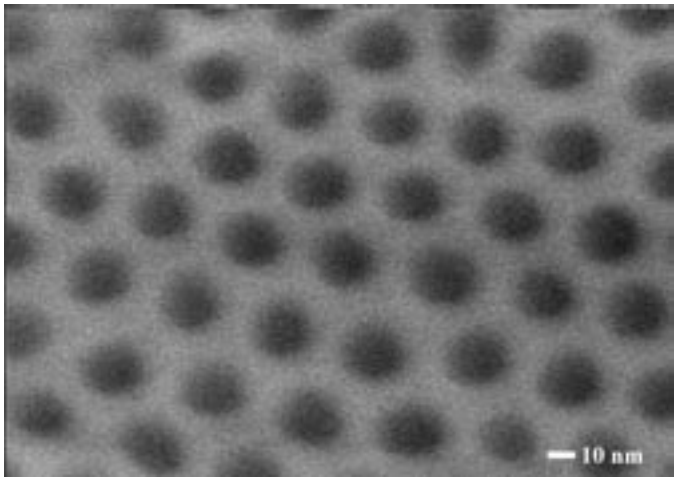

Fig. 19: SEM image of anodic alumina template with a 20nm diameter pore size.

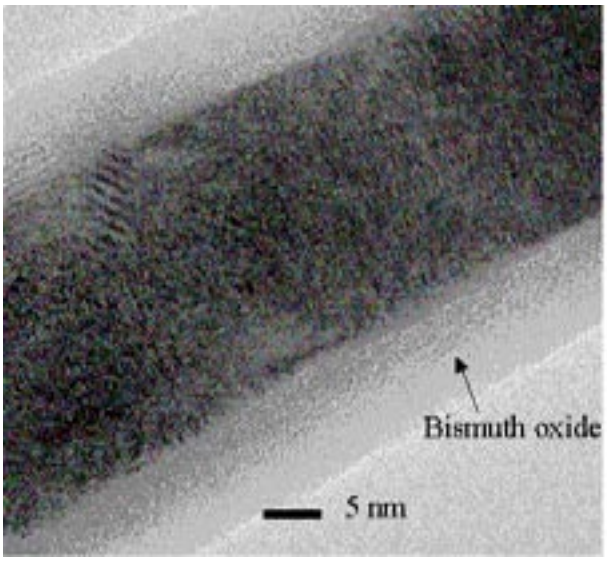

Fig. 20: HRTEM (high resolution transmission electron microscopy) image of a 25nm Bi nanowire with a 7nm thick oxide layer. The lattice fringes in the image indicate single crystalline Bi.

Nanomagnets

Personnel

M. Hwang, M. Farhoud, Y. Hao, M. Walsh, T. Savas, and E. Lyons
(C.A. Ross and H.I. Smith in collaboration with R. Ram, M. Abraham, F. Humphrey, R. Chantrell, and M. Redjdal)

Sponsorship

NSF and IBM Graduate Fellowship

We are using Interferometric Lithography (IL) in the NanoStructures Laboratory (NSL) of the Department of Electrical Engineering to produce large area arrays of 'nanomagnets' of period 100 - 200nm. These particles have been made by electrodeposition, by evaporation and liftoff, or by etching of a sputtered film. We are exploring the switching mechanisms of the particles, the thermal stability of their magnetization, and inter-particle interactions, and assessing their suitability for various data storage schemes. The collective behavior of the arrays can be measured using magnetometry and compared with the behavior of individual particles using magnetic force microscopy in order to understand how the behavior of one magnet is affected by its neighbors. From such data, the intrinsic variability between particles can be determined, and related to the microstructure. For instance, we found that the reversal in 30 nm-diameter polycrystalline Ni particles is governed by the grain structure.

We have also performed micromagnetic simulations to explore the remanent magnetic states, and mechanisms for magnetization reversal in these structures. Small particles have near-uniform magnetization states, while larger ones develop more complex structures such as magnetization vortices or domain walls. Good agreement between model and observed remanent states is obtained, taking the shape and crystal orientation into account.

These particle arrays have potential uses in 'patterned media', in which each particle stores one bit of data according to its magnetization direction.

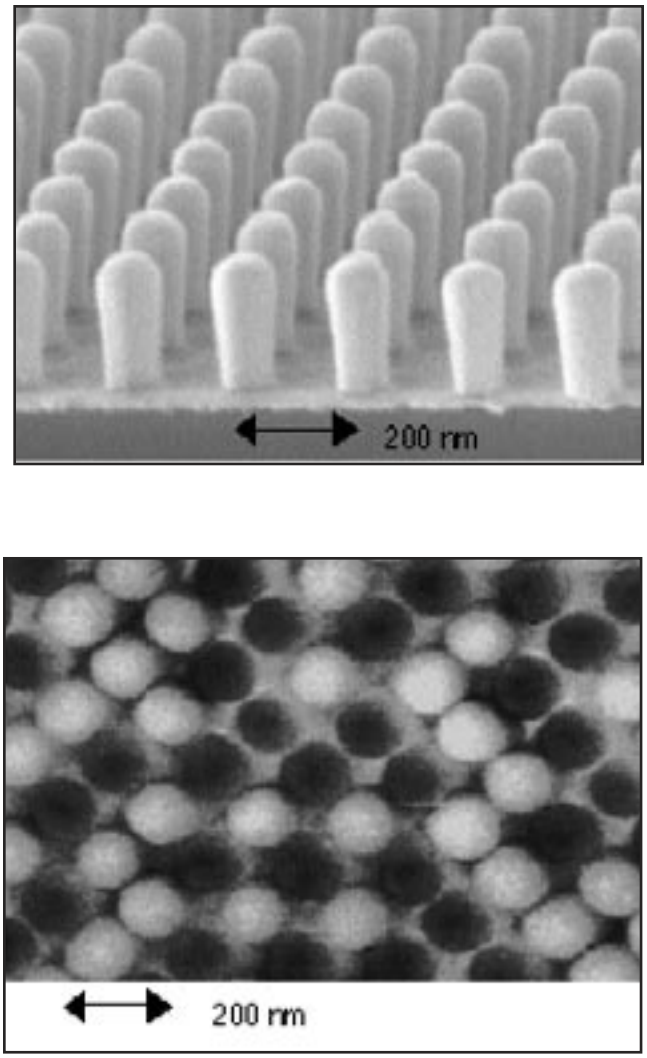

Fig. 21: An array of electrodeposited Ni pillars, with diameter 90 nm and height 220 nm. The magnetic image shows that each pillar is magnetized 'up' (light) or 'down' (dark).

Continued

Continued

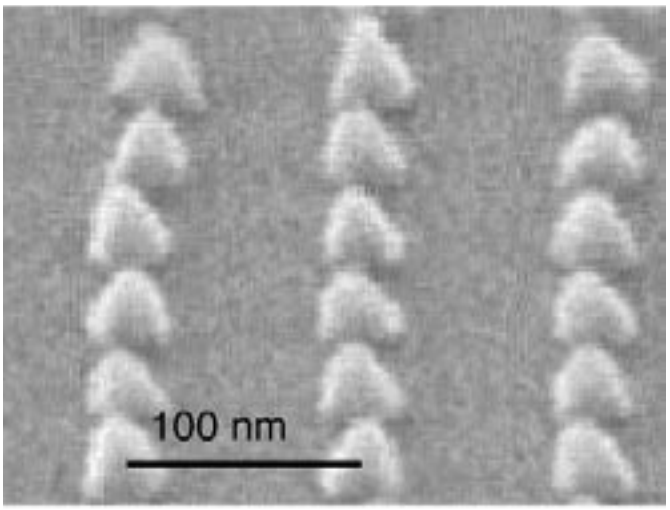

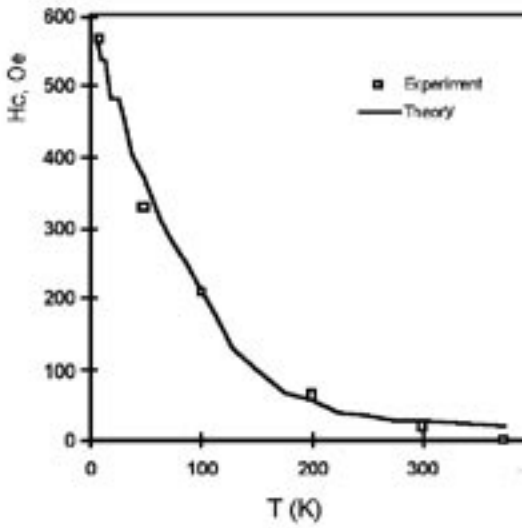

Fig. 22: An array of conical Ni particles made by evaporation. These have diameter 30 nm and period 100 nm. The magnetic properties are governed by the grain size, leading to superparamagnetic behavior at room temperature. At low temperatures the coercivity increases in agreement with a computational model.

Magnetic and Optical Films made by Pulsed Laser Deposition

Personnel

M. Shima, A.C. Ford, and T. Tepper
(C.A. Ross in collaboration with L.C. Kimerling)

Sponsorship

Nanovation, 3M Innovation Fund, IBM, and
MIT Materials Processing Center

We have established a Thin Film Laboratory which includes a Pulsed Laser Deposition (PLD) system and a UHV Sputter/analysis system. In PLD, a high energy excimer laser is used to ablate a target, releasing a plume of material which deposits on a substrate to form a thin film. PLD is particularly useful for making complex materials such as oxides because it preserves the stoichiometry of the target material. We have used PLD to produce films of Cr and CoCrPt alloys to compare with films produced by sputtering, in order to understand the importance of the plasma on film microstructure development, in particular the influence of energetic bombardment on the formation of the Cr (200) / CoCrPt (1120) preferred orientation. This will help in the design of hard-disk films based on a Cr underlayer. We have also been using PLD to deposit a variety of oxide films for photonic and magneto-optical devices.

Low Voltage Field Emitter Arrays by Aperture Scaling

Personnel
D. Pflug
(A. I. Akinwande, M. Schattenburg and H. I. Smith)

Sponsorship
DARPA

The objective of this project is to develop low voltage field emission arrays for application to small, high-resolution, high-luminous-efficiency and high-brightness display is the Field-Emitter-array flat-panel Display (FED). The FED incorporates a high density, high performance array of low-voltage field emitters to provide a display that has the viewing characteristics of a CRT in a thin light weight package. The low voltage arrays will allow CMOS-controlled electron emission from the tips. Low voltage FEAs will enable integration of the addressing and signal conditioning electronics on the same substrate as the Field Emitter Arrays (FEAs). This approach will result in the reduction of the number of wires and bond pads from about 2,000 to about 50. Our objective is to demonstrate the feasibility of fabricating low-voltage field-emitter arrays by scaling the gate aperture. Interferometric lithography is used to define field emitter arrays that are spaced 200 nm tip-to-tip and have <50 nm gate-to-emitter separation.
Our initial efforts focused on modeling the scaling behavior of FEA devices. Numerical simulation and computer models to predict FEA performance have been developed and continue to be refined. Simulation results indicate that we will be able to increase the current density and reduce the operating voltage, by decreasing the aperture to less than 100 nm.

FEAs of 200 nm period have been fabricated by using interferometric lithography and standard processing techniques. Additional metallization layers and conventional lithography were used to create discrete Molybdenum Spindt arrays for electrical characterization. The fabricated cones have similar size and structure to that simulated (Figure 24). Standard CMOS pro-

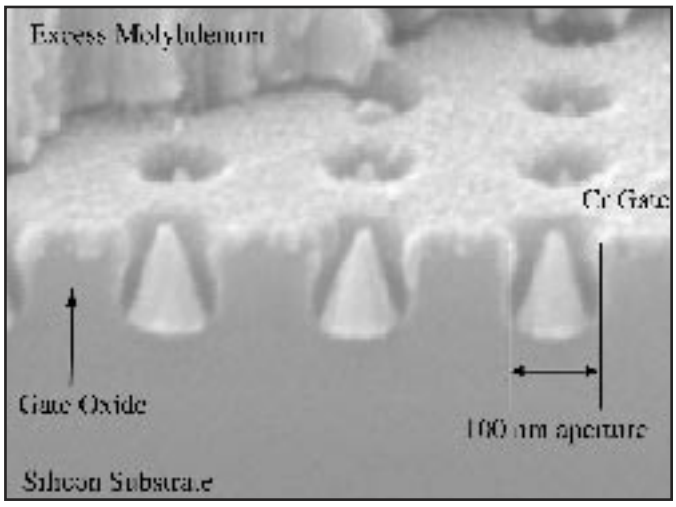

Fig. 24: 100 nm gate aperture molybdenum field-emitter cones with chromium gate formed using a vertical evaporation.

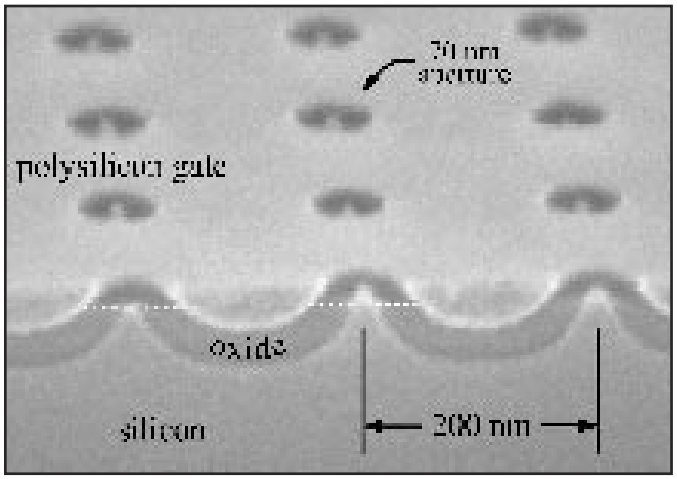

Fig. 25: 200 nm period, 70 nm aperture Silicon arrays with polysilicon gate. Formed by a rough cone formation, oxidation sharpening and CMP planarization.

Continued

cessing techniques have been also been combined with the interferometric lithography to form 200 nm period arrays of Si etched cones, (Figure 25).

Electrical characterization of the 100 nm aperture Molybdenum arrays (200 nm tip to tip spacing) has shown that arrays can operate at voltages as low as 16 volts and provide adequate current to support flat panel display applications. We have demonstrated initial testing of low-gate-voltage FEAs with discrete solid state devices by replacing the resistor that previous approaches have used to limit and control emission current with a discrete MOSFET. Current control is critical to the uniformity of brightness across the display because Fowler-Nordheim emission depends exponentially on the ratio of the gate voltage to the tip radius-of-curvature (Vg/r). It is therefore very sensitive to small changes in the radius-of-curvature. It was possible to control the emitted current density by three orders of magnitude using the gate voltage of the transistor.

Continued